Application of a Redundant Haptic Interface in Enhancing Soft-Tissue Stiffness Discrimination

Ali Torabi[1], Mohsen Khadem[2], Kourosh Zareinia[3], Garnette Roy Sutherland[4], Mahdi Tavakoli[1]

***Abstract*—Haptic-enabled teleoperated surgical systems have the potential to enhance the accuracy and performance of surgical interventions. The user interface of such a system can provide haptic feedback to the surgeon to more intuitively perform surgical tasks. In this paper, we study the added benefits of redundant manipulators as haptic interfaces for teleoperated surgical systems. First, we introduce the intrinsic benefits of employing a redundant haptic interface, namely, reduced apparent inertia and increased manipulability (one result of which is reduced friction forces). Next, we demonstrate that the haptic interface redundancy can further reduce its apparent inertia and friction via appropriately manipulating the extra degrees of freedom of the interface. This will consequently enhance the haptic feedback resolution (sensitivity) for the user. Finally, a psychophysical experiment is performed to validate the improved force perception for the user in a virtual soft-tissue palpation task. We conduct a set of perceptual experiments to evaluate how a redundant and non-redundant user interface affects the perception of the virtual stiffness. Experimental results demonstrate that the redundancy in the haptic user interface helps to enhance tissue stiffness discrimination ability of the user by reducing the distortions caused by the kinematics and dynamics of the user interface.**

***Index Terms*—Haptics and Haptic Interfaces, Telerobotics and Teleoperation, Medical Robots and Systems.**

I. Introduction

ROBOTIC teleoperation systems have transformed several surgical interventions, where many steps involved in localization, access, and surgical execution would benefit from distinct robotic capabilities. Teleoperated robotic systems combine the decision-making of human users with the precision of a robot, allowing minimalist intervention in confined spaces with accuracies beyond human capabilities [1]. One of the main capabilities of teleoperated robotic systems is providing haptic feedback to the surgeon. The haptic sense in telerobotics provides realistic interactions between a human user and a remote or virtual environment. To provide haptic feedback to the human user, there is a need for haptic interfaces that relay forces from the teleoperated robots interactions with the real or the virtual environment back to the human operator [2].

In a teleoperated robotic surgical system, the patient side surgical manipulators are controlled via a human interface (HI), operated by the surgeon. The HI connecting the surgeon to the surgical manipulator and environment is an integral part of any robot-assisted surgical system and should be able to intuitively transfer surgical maneuvers to the surgical robot [3], [4]. The HI should also provide sufficient sensory feedback such as haptic sense to the surgeon to more intuitively control the robotic manipulators. The haptic force feedback can reduce unintentional injuries [5], surgeon's fatigue [6], and assist tissue characterization [7].

For most surgical procedures, stiffness transparency is required to offer a realistic feel of the tissue [8]. Stiffness transparency allows surgeons to discriminate between tissues. Distorted haptic feedback can reduce the user's ability to perform tissue discrimination. Especially in neurosurgery, the user's tissue stiffness discrimination ability may be reduced due to small forces that are involved in the interaction with the brain tissue [9], which may be masked by the HI's mechanical properties.

In the design of HIs, there are trade-offs between desirable characteristics such as force feedback reflection capacity, closed-loop stiffness, workspace size, manipulability, and apparent inertia [10]. For example, to provide large force feedback, the HI should have larger actuators. This, however, increases the inertia of the robot and somewhat masks the force feedback. Also increasing the HI's workspace commonly leads to longer links, which decreases the mechanical stiffness and increases the inertia of the HI.

To address the design trade-offs and achieve desirable characteristics for HIs, one can use a kinematically redundant haptic interface (RHI). RHI has more degrees of freedom than what is minimally required to perform a task in the Cartesian space. Kinematic redundancy in the task space of a robot makes it possible to have joint motions that do not affect the position and orientation of the end-effector (EE). These inner joints' motions can be used in control to achieve a secondary objective while performing a primary objective. The secondary objective can involve reducing apparent inertia, singularity avoidance, manipulability enhancement, and/or joint limit avoidance [11].

Despite the promising features of RHIs, not much attention has been paid to its design and control. One of

Manuscript received: September, 10, 2018; Revised December, 1, 2018; Accepted December, 29, 2018.

This paper was recommended for publication by Editor Allison M. Okamura upon evaluation of the Associate Editor and Reviewers' comments. This research was supported by the Canada Foundation for Innovation (CFI) under grant LOF 28241, the Alberta Innovation and Advanced Education Ministry under Small Equipment Grant RCP-12-021, the Natural Science and Engineering Research Council (NSERC) of Canada under the Collaborative Health Research Projects (CHRP) Grant, and the Quanser, Inc.

[1]A. Torabi and M. Tavakoli are with the Department of Electrical and Computer Engineering, University of Alberta, Edmonton, AB, Canada. {ali.torabi, mahdi.tavakoli}@ualberta.ca

[2]M. Khadem is with the School of Informatics, University of Edinburgh, Edinburgh, UK. mohsen.khadem@ed.ac.uk

[3]K. Zareinia is with the Department of Mechanical Engineering, Ryerson University, Toronto, ON, Canada. kourosh.zareinia@ryerson.ca

[4]G. Sutherland is with the Project neuroArm, Faculty of Medicine, University of Calgary, Calgary, AB, Canada. garnette@ucalgary.ca

Digital Object Identifier (DOI): see top of this page.

the first redundant haptic interfaces was introduced in [12]. They proposed an admittance controller to control the robot due to its relatively large dynamics that make the HI non-backdriveable. Nath et al. [13] studied the teleoperation of redundant manipulators when both the master and slave robots are redundant and have the same degrees of freedom. Barrow et al. [14] and Gosselin et al. [15] added one degree of freedom (DoF) to the base of the HIs to make the robots kinematically redundant and enlarge their workspaces. The well-known da Vinci Surgical System (Intuitive Surgical, Inc. CA, USA) also benefits from a redundant 7-DoF Master robot [16]. The rest of the work found in literature considers the case of a redundant teleoperated robot (slave robot). Hwang et al. [17] studied the performance of a teleoperation robotic system that benefits from a redundant slave robot manipulator. Das et al. [18] developed a kinematic controller for a teleoperation system with a redundant slave robot system. They performed obstacle avoidance while controlling the robot in its task-space.

In this paper, we investigate the benefits of an RHI as the master robot in a tissue discrimination scenario. We employ an RHI to reduce the apparent inertia of the interface and enhance its manipulability and consequently enhance the force resolution (sensitivity) for the user. We demonstrate that an RHI can provide better and more realistic force feedback to the user than a non-redundant haptic interface (NHI). The rest of the paper is organized as follows: In Section II, the intrinsic advantages of an RHI over NHI is described. In Section III, a secondary task is introduced that employs the kinematic redundancies of the RHI to further maximize its manipulability in the desired direction. Section IV describes the experimental setup and protocol. Psychophysical experiment results to validate the effectiveness of the proposed secondary task and redundancy of the haptic interface are presented in Section V. Concluding remarks appear in Section VI.

II. Intrinsic Advantages of Redundant Haptic Interfaces

A haptic interface should satisfy requirements of low apparent inertia and friction for the best perception of reflected forces by the user, a big workspace for ease of movement, and a large enough stiffness and maximum force feedback capability to recreate reflected forces from both soft and stiff contacts. In this section, we show the intrinsic advantages (i.e., enhanced manipulability and lower apparent inertia) of a redundant haptic interface (RHI) over a non-redundant interface (NHI). An RHI has intrinsic advantages over an NHI as long as the RHI has at least one DoF more than the NHI. Intrinsic advantages are related to the kinematics and dynamics of the RHI and do not need any algorithm or computer-based control. In Section III, we demonstrate that by employing an RHI, the intrinsic advantages of an RHI can be more enhanced via a secondary task controller.

A. Effective Manipulability

For a robot, the Jacobian matrix provides a transformation from the joint velocities to the velocity of the EE in Cartesian space as

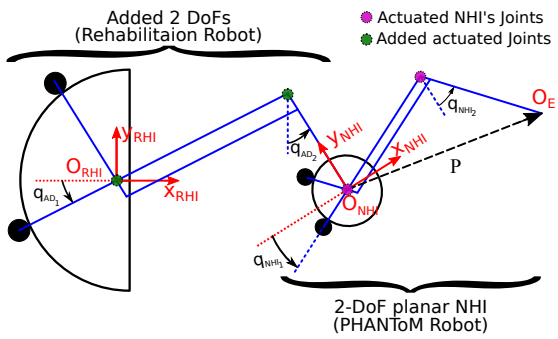

Figure 1. Schematics of a 4-DoF planar RHI.

$$\dot{x} = \begin{bmatrix} \dot{t} \\ \dot{r} \end{bmatrix} = \begin{bmatrix} J_t \\ J_r \end{bmatrix} \dot{q} = J\dot{q} \tag{1}$$

where $\dot{q}$ is an n-dimensional vector that represents a set of joint velocities, $\dot{x}$ is an m-dimensional velocity vector of the EE, and J is the $m \times n$ Jacobian matrix. $\dot{t}$ is a t-dimensional translational velocity vector, and $\dot{r}$ is an r-dimensional orientational velocity vector of the EE. J_t and J_r are the $t \times n$ translational and $r \times n$ orientational Jacobian matrices, respectively. For the RHI, $n > m$, and for the NHI, $n = m$.

For a given robot, a unit hypersphere in the joint space, $\|\dot{q}\|^2 = 1$, can be mapped into an ellipsoid in Cartesian space, using [19]

$$\|\dot{q}\|^2 = \dot{q}^T\dot{q} = \dot{x}^T(J^\dagger)^T(J)^\dagger\dot{x} = \dot{x}^T(JJ^T)^\dagger\dot{x} = \dot{x}^T\mathcal{M}\dot{x} \tag{2}$$

where $\dagger$ indicates the pseudo-inverse of a matrix and $\mathcal{M}$ is an $m \times m$ matrix and called the velocity manipulability ellipsoid (VME). The VME is a useful tool for visualizing the velocity transmission characteristics of a manipulator at a given configuration. The optimal direction for affecting velocity as well as the optimal direction to control the force is along the major axis of the VME [20]. This means that for an HI, along the major axis of the VME, the user can move the EE with minimum movements of the robot's joints (i.e., feeling the least joint frictions). Also, along with the major axis of the VME, the force feedback to the user can be most accurately controlled (i.e., the highest resolution of force feedback).

The effective manipulability for VME along the direction of a unit vector u is calculated as [20]

$$\rho = (u^T\mathcal{M}u)^{-1/2}, \tag{3}$$

ρ takes its maximum along the major axis of the VME.

Consider an RHI which is made by adding one or more DoFs to the base of an NHI. An example of an RHI is illustrated in Fig. 1. Let P represent the vector connecting the origin of the NHI, O_{NHI}, to the origin of the EE, O_E, expressed in the reference frame attached to the origin of the RHI, O_{RHI}. Consider $\dot{t}_{NHI}$ and $\dot{r}_{NHI}$, which represents the translational and angular velocities of the origin of the NHI, O_{NHI}, as the result of the motion of the added DoFs, and $\dot{t}_E$ and $\dot{r}_E$, which represents the translational and angular velocities

of the EE, O_{E}, as the result of the motion of the NHI. The Jacobian matrix of the RHI can be calculated as

$$\begin{aligned}\begin{bmatrix}\dot{t}\\ \dot{r}\end{bmatrix} &= \begin{bmatrix}\dot{t}_{NHI}+\dot{t}_{E}+\dot{r}_{NHI}\times P\\ \dot{r}_{NHI}+\dot{r}_{E}\end{bmatrix}\\ &= \begin{bmatrix}J_{t_{AD}}-[P]_{\times}J_{r_{AD}} & J_{t_{NHI}}\\ J_{r_{AD}} & J_{r_{NHI}}\end{bmatrix}\begin{bmatrix}\dot{q}_{AD}\\ \dot{q}_{NHI}\end{bmatrix}\\ &= \left[\begin{bmatrix}I & -[P]_{\times}\\ 0 & I\end{bmatrix}\begin{bmatrix}J_{t_{AD}}\\ J_{r_{AD}}\end{bmatrix}\quad\begin{bmatrix}J_{t_{NHI}}\\ J_{r_{NHI}}\end{bmatrix}\right]\begin{bmatrix}\dot{q}_{AD}\\ \dot{q}_{NHI}\end{bmatrix}\\ &= \left[\begin{bmatrix}I & -[P]_{\times}\\ 0 & I\end{bmatrix}J_{AD}\quad J_{NHI}\right]\begin{bmatrix}\dot{q}_{AD}\\ \dot{q}_{NHI}\end{bmatrix}\\ &= \begin{bmatrix}\hat{J}_{AD} & J_{NHI}\end{bmatrix}\begin{bmatrix}\dot{q}_{AD}\\ \dot{q}_{NHI}\end{bmatrix} = J_{RHI}\dot{q}_{RHI}\end{aligned} \tag{4}$$

where $[P]_{\times}$ is the cross-product operator of the vector P. $\dot{q}_{AD}$ and $\dot{q}_{NHI}$ are the joint velocity vectors corresponding to the added DoFs and NHI, respectively. J_{AD} and J_{NHI} are the Jacobian matrices of the added DoFs and NHI which are expressed in the frame attached to the origin of the RHI, and J_t and J_r are the translational and orientational parts of the Jacobian matrices. I and 0 are the identity and null matrices, respectively, with appropriate dimensions.

Remark I: By adding one or more DoFs to the base of an NHI to make it redundant, the effective manipulability of the new redundant robot will be greater than that of the NHI.

For the RHI, the effective manipulability (3) along a direction u can be written as

$$\begin{aligned}\rho_{RHI} &= (u^{T}(J_{RHI}J_{RHI}^{T})^{\dagger}u)^{-1/2}\\ &= (u^{T}(\begin{bmatrix}\hat{J}_{AD} & J_{NHI}\end{bmatrix}\begin{bmatrix}\hat{J}_{AD}^{T}\\ J_{NHI}^{T}\end{bmatrix})^{\dagger}u)^{-1/2}\\ &= (u^{T}(\hat{J}_{AD}\hat{J}_{AD}^{T}+J_{NHI}J_{NHI}^{T})^{\dagger}u)^{-1/2}.\end{aligned} \tag{5}$$

As the VME belongs to the set of symmetric positive definite (SPD) matrices, it can be shown that

$$u^{T}(\hat{J}_{AD}\hat{J}_{AD}^{T}+J_{NHI}J_{NHI}^{T})^{\dagger}u \leq u^{T}(J_{NHI}J_{NHI}^{T})^{\dagger}u, \tag{6}$$

and thus,

$$\rho_{RHI} \geq \rho_{NHI}. \tag{7}$$

The inequality (7) shows that the effective manipulability for the RHI is greater than that for the NHI in any direction. Therefore, the user would feel less joint friction when he/she moves the EE of the RHI.

B. Effective Apparent Inertia

Remark II: The effective apparent inertia of the RHI, which is made by adding one or more DoFs to the base of an NHI, is smaller than that of the NHI.

The effective apparent inertia describes the relationship between a force (torque) applied on the EE of the robot along (about) an arbitrary direction and its resulting translational (rotational) acceleration in that direction, taking into account the effects of the other links and joints of the robot. In other words, effective apparent inertia represents the mass perceived at the EE of the robot in response to the applied force (torque) along (about) an arbitrary direction.

The apparent inertia of an HI (redundant or non-redundant) can be written as $M_x = (JM_q^{-1}J^{T})^{-1}$ [21], where M_x is the $m\times m$ EE inertia matrix in Cartesian space (apparent inertia), and M_q is the $n\times n$ inertia matrix in the joint space. The inertia matrix of the RHI is shown to be [22]

$$M_{q,RHI} = \begin{bmatrix}M_{q,AD} & \hat{M}_q\\ \hat{M}_q^{T} & M_{q,NHI}\end{bmatrix} \tag{8}$$

where $M_{q,AD}$ is the inertia matrix of the added DoFs, $\hat{M}_q$ is the co-term of the inertia matrix of the added DoFs and NHI, and $M_{q,NHI}$ is the inertia matrix of the NHI. The terms in (8) are expressed in the RHI reference frame. The apparent inertia of the RHI is calculated as

$$M_{x,RHI} = (J_{RHI}M_{q,RHI}^{-1}J_{RHI}^{T})^{-1} = (M_{x,NHI}^{-1}+\hat{M}_x^{-1})^{-1} \tag{9}$$

where J_{RHI} is calculated from (4),

$$\hat{M}_x^{-1} = (\hat{J}_{AD}-J_{NHI}M_{q,NHI}^{-1}\hat{M}_q)(M_{q,AD}-\hat{M}_q^{T}M_{q,NHI}^{-1}\hat{M}_q)^{-1}$$
$$(\hat{J}_{AD}-J_{NHI}M_{q,NHI}^{-1}\hat{M}_q)^{T}, \text{and}\quad M_{x,NHI}^{-1} = (J_{NHI}M_{q,NHI}^{-1}J_{NHI}^{T}).$$

The effective apparent inertia in the direction u is calculated as

$$\Lambda = (u^{T}M_x^{-1}u)^{-1}. \tag{10}$$

Therefore, the effective apparent inertia of the RHI can be calculated as

$$\Lambda_{RHI} = (u^{T}M_{x,RHI}^{-1}u)^{-1} = (u^{T}M_{x,NHI}^{-1}u+u^{T}\hat{M}_x^{-1}u)^{-1}. \tag{11}$$

As $(u^{T}\hat{M}_x^{-1}u)$ is always positive [22], thus

$$(u^{T}M_{x,RHI}^{-1}u)^{-1} \leq (u^{T}M_{x,NHI}^{-1}u)^{-1}. \tag{12}$$

The inequality (12) indicates that the effective apparent inertia of the RHI is smaller than that of the NHI along any direction.

III. Non-Intrinsic Advantages of Redundant Haptic Interfaces

In Section II, the intrinsic advantages of the RHI over NHI were investigated. In this section, the redundancy of the RHI will be exploited to achieve a secondary objective. In Section IV, we experimentally validate the application of the proposed approach in enhancing the soft-tissue discrimination by using an RHI.

For an RHI, the joint torque vector for a desired EE force can be calculated as [21]

$$\tau = J^{T}F + \underbrace{(I-J^{T}J^{\#^{T}})(\tau_N - k_D\dot{q})}_{\text{Null space controller}}, \tag{13}$$

where τ is the joint torque vector required to create a desired EE force F. τ_N is the null-space torque vector corresponding to the secondary objective and is projected in the null space of the Jacobian matrix through the $(I-J^{T}J^{\#^{T}})$ matrix. $k_D>0$ is a suitable damping coefficient. $J^{\#}$ is generalized inverse of the Jacobian matrix defined as $J^{\#} = M_q^{-1}J^{T}[JM_q^{-1}J^{T}]^{-1}$. The joint torques given by (13) can ensure stability for both the primary and null space controllers [23]. A block diagram of the control system is shown Fig. 2.

The torque vector, τ_N, which is desired to fulfill secondary goals needs to optimize a secondary objective using the gradient projection method, i.e.,

$$\tau_N = -\alpha\frac{\partial\nu(q)}{\partial q} \tag{14}$$

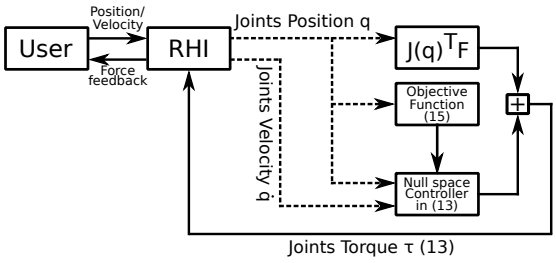

Figure 2. Block diagram of the control system.

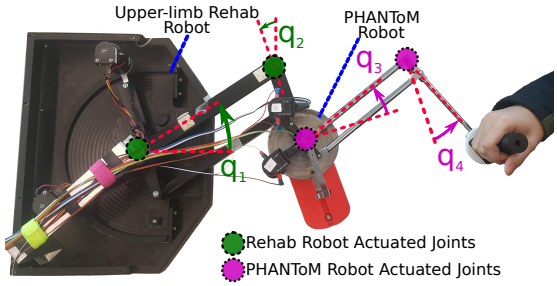

Figure 3. Top view of experimental Setup (4-DoF planar RHI). The first NHI (PHANToM) is made by fixing $q_1 = 0$ and $q_2 = 0$. The second NHI (Rehab) is made by fixing $q_3 = 0$ and $q_4 = 0$.

where α is a scalar step size and $\nu(q)$ is the objective function corresponding to the secondary task. Using τ_N in (14), the robot tries to decrease the value of $\nu(q)$ while executing the primary task.

As discussed in Section I, different secondary objectives can be selected. An ideal HI is such that the user does not sense the dynamics of the HI. This can be achieved by maximizing the manipulability of the HI and minimizing its apparent inertia along the desired direction of motion. We note that by designing a suitable closed-loop controller (e.g., impedance control [24]) for the HI, the apparent inertia can be decreased and the joints' friction can be compensated for. However, such controller needs an exact model of the HI joints friction, inertia matrix and centrifugal torques in addition to a force sensor that are hard to achieve in practical applications. Therefore, having intrinsic low apparent inertia and friction, and high manipulability is desirable for HIs.

We define an objective function for the secondary task to match the VME of the RHI, $\mathcal{M} = (J_{RHI} J_{RHI}^T)^\dagger$, to a desired VME, $\mathcal{M}_{des}$, by utilizing the inner joints motion of the redundant robot. The objective function is defined as

$$\nu(q) = \texttt{logdet}\left(\frac{\mathcal{M}_{des} + \mathcal{M}}{2}\right) - \frac{1}{2}\texttt{logdet}(\mathcal{M}_{des}\mathcal{M}). \quad (15)$$

As stated before, $\mathcal{M}$ belongs to the set of SPD matrices. (15) is selected as the cost function because it is a Riemannian distance metric on SPD matrices [25] and forms a convex optimization problem that ensures convergence. $\mathcal{M}_{des}$ is designed such that its major axis is aligned to the desired direction of motion and it has small minor axes. By using this $\mathcal{M}_{des}$, the effective manipulability will be maximized along the desired direction. If $u \in R^m$ is the unit vector that indicates the direction of motion, by using singular value decomposition (SVD), it can be decomposed as $u = U\Sigma V^T$, where U is $m \times m$ unitary matrix, Σ is an $m \times 1$ vector in which non zero value is known as the singular value of u, and V is a scalar.

The desired VME can be defined as

$$\mathcal{M}_{des} = U \begin{bmatrix} \Sigma, & \begin{bmatrix} 0_{1\times(m-1)} \\ \beta I_{(m-1)} \end{bmatrix} \end{bmatrix} U^{-1} \quad (16)$$

where $I_{(m-1)}$ is an $(m-1)\times(m-1)$ identity matrix, $0_{1\times(m-1)}$ is a vector of zeroes. β is a scalar scaling factor that defines the length of the minor axes of the $\mathcal{M}_{des}$. In theory, an ideal $\mathcal{M}_{des}$ is a line (i.e. $\beta = 0$); however, such a desired VME causes an internal motion that puts the HI into a singular configuration. Therefore, the parameter β needs to be small but non-zero to avoid singularity in any direction.

In the cost function (15), the effective manipulability (3) is maximized along the desired direction of motion. Also, there is control over the desired VME shape in the cost function (15), and thus singularities can be prevented by selecting an appropriate value for β. Furthermore, this cost function forms a convex optimization problem. Therefore, the optimization converges to the global solution of the problem and does not depend on the initial configuration of the robot.

IV. Experimental Setup and Protocol

Here, the effect of the proposed control strategy on the performance of the user in soft-tissue stiffness discrimination is investigated. Using three robots – two planar 2-DoF NHIs and a planar 4-DoF RHI – a user study is performed. The experiments aim to study user perception of changes in stiffness. Based on the discussions in Section III, it is hypothesized that because the RHI has lower effective apparent inertia and larger effective manipulability, which as a result, has higher force feedback accuracy compared to the NHIs, the RHI can enhance the soft-tissue stiffness discrimination ability of a user.

The 4-DoF planar RHI is developed by serially connecting two robots, a 2-DoF PHANToM 1.5A (Geomagic Inc., Morrisville, NC, USA) and a 2-DOF planar upper-limb rehabilitation robot (Quanser Inc., Markham, ON, Canada). The base joint of the 3-DoF PHANToM robot has been removed to turn it into a 2-DoF planar robot. Also, a passive revolute joint is added to the EE of the 4-DoF RHI to allow for any arbitrary orientation of the user's hand. For interfacing the robots with the computer, MATLAB/Simulink (MathWorks Inc., Natick, MA, USA) with Quarc real-time control software (Quanser Inc., Markham, ON, Canada) is used.

The experimental setup is shown in Fig. 3. One of the NHIs is made by fixing the first two joint angles of the RHI at zero, i.e., upper-limb rehabilitation robot's joints (q_1 and q_2) are set to zero. The second NHI is made by fixing the last two joint angles of the RHI at zero, i.e., PHANToM robot's joints (q_3 and q_4) are set to zero. The first NHI's kinematics and dynamics are equivalent to the PHANToM robot's kinematics and dynamics and will be called PHANToM hereafter, and the second NHI's kinematics and dynamics are comparable to the rehabilitation robot's kinematics and dynamics and will be called Rehab hereafter.

The Jacobian matrix of the RHI, PHANToM, and Rehab are

$$J_{RHI} = \begin{bmatrix} -d_1 sq_1, & d_2 cq_2 - d_3 sq_{23} + d_4 cq_{24}, & -d_3 sq_{23}, & d_4 cq_{24} \\ d_1 cq_1, & d_2 sq_2 + d_3 cq_{23} + d_4 sq_{24}, & d_3 cq_{23}, & d_4 sq_{24} \end{bmatrix},$$

$$J_{PHANToM} = \begin{bmatrix} -d_3 sq_3, & d_4 cq_4 \\ d_3 cq_3, & d_4 sq_4 \end{bmatrix},$$

$$J_{Rehab} = \begin{bmatrix} -d_1 sq_1, & (d_2 + d_4) cq_2 - d_3 sq_2 \\ d_1 cq_1, & (d_2 + d_4) sq_2 + d_3 cq_2 \end{bmatrix},$$

where q_i, $i = 1, 2, 3, 4$, is the HIs joint angles, s and c denote $sin(.)$ and $cos(.)$, and $q_{ij} = q_i + q_j$. The links' length of the HIs are given in meters as $d_i = [0.254,\ 0.141,\ 0.21,\ 0.181]$. The inertia matrix in the joint space for the RHI, PHANToM, and Rehab are obtained based on the work of [26] and [27].

Ten subjects aged 22-33 participated in the experiments. The subjects had average experience with HIs, and all of them were right-handed. Each subject was asked to sit in front of an HI and move the EE of the HI with their dominant hand in a given direction and receive haptic feedback form a virtual environment without having any visual feedback. Subjects were instructed to keep the EE of the HI moving during the experiments. Before starting the experiments, the subjects performed a round of training to become familiar with the experimental setup. The experiment was approved by the University of Alberta Research Ethics and Management Online under study ID MS3_Pro00057919.

A psychophysical experiment is performed to study the users' perception of changes in stiffness. The two-alternative forced-choice (2AFC) procedure, which forces the subjects to choose which stimuli in a pair of reference and comparison sample is stiffer, was employed in each trial. Also, the method of constant stimuli [28], in which a reference stimulus and a set of comparison stimulus are presented to the subject in the random order, is used. The virtual environment is modelled by a spring whose stiffness changes by the stimulus value.

The subjects' primary goal was distinguishing between different virtual stiffnesses. In each trial, one of the haptic interfaces (RHI, PHANToM, or Rehab) and pairs of virtual tissue samples (virtual stiffnesses) were presented to the subject. Each pair consists of a reference stimulus value and a comparison stimulus value. The reference value was selected to be in the lower band of the brain tissue stiffness. The Young's modulus of brain tissue is 0.6 to 180kPa [29]. By using Hooke's law, Young's modulus is converted to the spring stiffness. Therefore, the stiffness values for a cube of the tissue sample with a length of $8\ cm$ is in the range of 50 to 14,500 N/m. Here, the reference stimulus value was selected to be 50 N/m, which is the lowest in the range for the brain tissue. The minimum stiffness for the brain tissue has been selected as the reference stimuli because it corresponds to very small forces that can be obscured by the mechanical impedance (including apparent inertia) and joint frictions of the HI [30]. Larger stiffnesses that correspond to forces overshadowing such dynamical effects are indeed easier for the human user to feel. Thus, the most challenging case for the human user (feeling and discriminating small stiffnesses) has been chosen to investigate the effectiveness of RHIs in terms of enhancing stiffness discrimination capabilities for human users compared to NHIs.

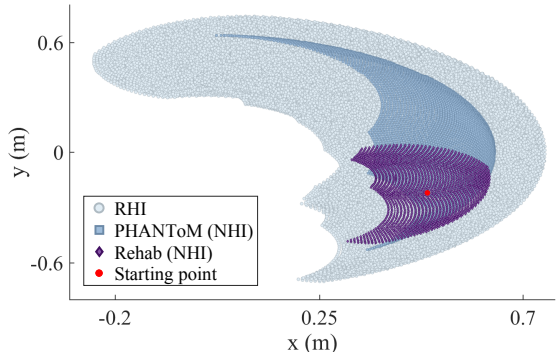

Figure 4. The workspace of the redundant robot, the workspace of the PHANToM, the workspace of the Rehab, and the starting point for the experiments.

A total of nine comparison values were selected so that four comparison values were smaller than the reference, four were larger than the reference, and one was equal to the reference. The comparison values selected are $\pm 5\%$, $\pm 15\%$, $\pm 25\%$, and $\pm 35\%$ of the reference stimulus value. In each trial, a pair of reference virtual stiffness and a virtual tissue sample from the comparison set was presented to the user. The user was asked to probe the first virtual tissue sample from the pair in the given direction. After the virtual tissue sample was probed, it was replaced by the other virtual tissue sample from the pair upon the subject's verbal signal concerning his/her readiness.

For each HI, the nine pairs of reference and comparison virtual stiffnesses were presented ten times in random orders to the subjects. Therefore, a total of 90 stiffness comparisons with each HI (270 comparisons in total) were made by the subjects. There was no time limit for probing the virtual stiffnesses in each trial. However, a physical obstacle is placed at $8\ cm$ away from the starting point of the experiments to limit the range of the EE movement. If the range of motion was not limited, as the virtual tissues follow the Hooke's law, the users could move the EE of the HI farther and discriminate the tissues by feeling the extra forces. Also, to ensure that the participants move their hand in a specific direction, a virtual fixture (software-generated force fields) is imposed on the EE of the HIs to limit the movement of the EE along the specific direction. The subjects were asked to always choose the stiffer tissue sample in a pair even if such a choice appeared challenging. To reduce the effects of fatigues in the experiments, the subjects had ten minutes optional rest time after every 45 comparisons. Also, after every 135 comparisons, the subjects had to have at least one hour rest.

The study was performed with the EE always starting from a point in the middle of the PHANToM workspace, $(0.49,\ -0.22)$, which is then moved in the right-hand direction (i.e., $u = [0,\ 1]^T$) towards the tissue . Fig. 4 depicts the workspace of the RHI, PHANToM and Rehab, and the location of the starting point in the workspaces. The base frame of the RHI and Rehab is located at $(0,\ 0)\ m$ and the base frame of PHANToM is located at $(0.254,\ -0.141)\ m$.

As proven in Remark I in Section II, the effective manipulability of the RHI is greater than or equal to that of the PHANToM at every point of its workspace. Also, as proven

Table I. Theoretical values for effective apparent inertia Λ and effective manipulability ρ at two points

	Point	RHI	PHANToM	Rehab
Λ (Kg)	(0.49, -0.22)	0.0576	0.0628	0.4379
	(0.49, -0.14)	0.0590	0.0606	0.4414
ρ (m/s)	(0.49, -0.22)	0.371	0.188	0.296
	(0.49, -0.14)	0.387	0.167	0.315

in Remark II in Section II, the effective apparent inertia of the RHI is upper bounded by that of the PHANToM at every point of its workspace. This means that the apparent inertia of the RHI is smaller than the PHANToM's apparent inertia, despite the fact that the RHI has two more links and actuators (resulting to the bigger workspace shown in Fig. 4). Therefore, it can be expected that the RHI provides higher fidelity force feedback for the user compared to the PHANToM because the RHI's mechanical properties mask the force feedback less than those of the PHANToM. To further investigate this, the effective manipulability and apparent inertia along $u = [0,\ 1]^T$ for the RHI, PHANToM, and Rehab are calculated at two points using (3) and (10), respectively. The perceptual experiments are performed for a line segment with these two points as its extremes. Results are listed in Table I. Data reported for the RHI in Table I corresponds to the optimized configuration of the RHI with the objective function given in (15). Parameter β in (16) is selected equal to 0.01 in the simulation studies and the experiments. The optimized configuration for the RHI at point $(0.49,\ -.22)\ m$ is $[0.125,\ 0.022,\ 0.298,\ 0.175]$ rad, and the optimized configuration at point $(0.49,\ -0.14)\ m$ is $[0.298, 0.077, 0.413, 0.208]$ rad.

Table I indicates that at sample points in the shared workspace of the RHI, PHANToM, and Rehab, the effective apparent inertia Λ in a specific direction for the RHI is smaller than that of the PHANToM and Rehab, although the effective manipulability ρ for the RHI is larger than that of the PHANToM and Rehab. Having a smaller apparent inertia for the RHI leads to the smaller sensation of its linkages, and having a larger effective manipulability for the RHI leads to the smaller sensation of its joints' frictions, both of which are desirable features.

Experiments are performed to validate the effective apparent inertia of HIs reported in Table I along $u = [0,\ 1]^T$. For this purpose, a 6-DoF force sensor (50M31A3-I25, JR3 Inc., Woodland, CA, USA) is attached to the EE of the HI. Next, the EE of each HI is modelled to have the dynamics

$$\Lambda \ddot{X} + F_r = F_{ext}, \tag{17}$$

where Λ is the scalar mass or effective apparent inertia in the direction of motion, X is the scalar position of the EE, F_{ext} is the scalar external force, and F_r is the scalar friction force. The friction term is modelled as the viscous friction $F_r = B\dot{X}$. Experiments are performed to identify Λ and F_r in (17). For each HI, ten trials are conducted. In each trial, a constant external force is applied to the EE of the HI along the direction of u starting at 1 cm before the points given in Table I in the workspace. The starting point is not chosen at the given points to eliminate the effects of Coulomb friction in the experiments. The acceleration and velocity of the EE of each HI as well as the external forces are measured. In the experiments, the HIs' joint angles are measured and by using forward kinematics of the HIs, the position of the EE is calculated. The velocity and acceleration of the EE are obtained by taking the first and the second derivative of the position of the end-effector using a second order filter, respectively. The external forces are exerted in the range of $0.5 - 1.5\ N$. The measured signals are passed through a 5th-order lowpass filter, and then the parameters are identified by fitting experimental data to (17) using linear least-squares method. The experimental results for the effective apparent inertia are listed in Table II. These experimental results are in agreement with the theoretical results in Table I. There is a small difference between the theoretical and experimental values which could be the result of measurement noises and model uncertainties, but the trend of apparent inertia value changes between the three HIs is consistent.

Table II. Experimental values for effective apparent inertia Λ in the right direction at two points

	Point	RHI	PHANToM	Rehab
Λ (Kg)	(0.49, -0.22)	0.0691	0.0734	0.5399
	(0.49, -0.14)	0.0718	0.0728	0.5683

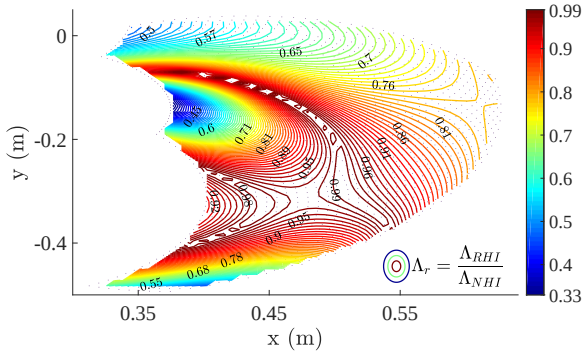

Figure 5. Effective apparent inertia ratio of the RHI and PHANToM.

In addition to the theoretical values reported in Table I, a simulation study is performed to verify Remark II in Section II in all points of the common workspace of the RHI and the PHANToM (NHI). (12) is re-written as $\Lambda_r = \frac{\Lambda_{RHI}}{\Lambda_{NHI}} \leq 1$, where Λ_r is the effective apparent inertia ratio. Theoretical values for the Λ_r along $u = [0,\ 1]^T$ are calculated at every point of the common workspace of the RHI and the PHANToM. Results are depicted in Fig. 5 which corroborate Remark II statement.

V. Results and Discussion

In order to quantify the users' perception of changes in stiffness in the experiments, we employed the just noticeable difference (JND), the point of subjective equality (PSE), and corresponding Weber Fractions (WF) measures. The JND is the minimum amount by which stiffness value must be altered to make a noticeable change in the user's perception. The PSE

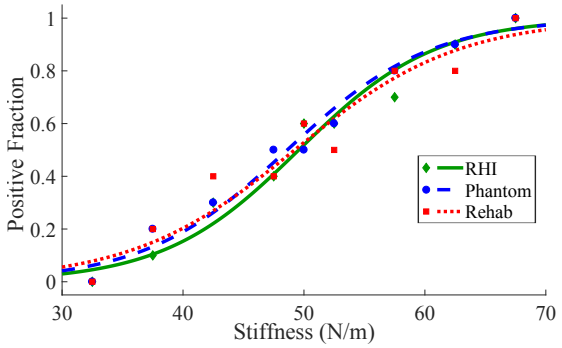

Figure 6. Representative results of the positive fraction for subject #3.

is the stiffness stimuli that appears to subjects the same as reference stiffness stimuli. The Weber fraction is calculated as

$$WF = \frac{JND}{PSE}. \tag{18}$$

Weber's Law states that the JND is a constant proportion of the original stimulus value.

A Sample of representative results of the positive fraction for each HI for subject #3 are shown in Fig. 6. The positive fraction is defined as the percentage of times each subject stated that the comparison stimuli value was stiffer than the reference stimuli value. A Psychometric function was fitted to each subjects' positive fraction data using the Psignifit Toolbox version 2.5.6 for MATLAB [31]. PSE, the upper threshold (UT) (where 75% of the responses report stiffer stimuli), and the lower threshold (LT) (where 25% of the responses report stiffer stimuli) are extracted from the fitted curve for each subject. The JND is defined as the half of the interval between UT and LT, which can be written as

$$JND = \frac{UT - LT}{2}. \tag{19}$$

The box graphs in Fig. 7(a) and Fig. 7(b) depict the mean and median values of the WF and JND for the three HIs, respectively. The experiments results are summarized in Table III. When compared to the previous stiffness discrimination studies using NHIs, the WFs for all three HIs are in a typical range (the stiffness WFs reported ranging from 0.08 to 0.30 [32]–[34]). The mean value for the WF and JND for the tissue stiffness discrimination with RHI are smaller than that with PHANToM and Rehab. This shows the effectiveness of the proposed redundant interface. To further inspect this, a one-way ANOVA test was applied to the WF data ($F(2, 27) = 7.36, P = 0.0032$), which indicates the statistically significant difference between three HIs. For more accurate analysis, the paired-sample t-test on the WF data is used between different pairs of HIs. The P-values are adjusted with the Holm–Bonferroni method. The t-test between RHI and PHANToM shows no statistically significant difference ($P = 0.2958$). However, the t-tests between RHI and Rehab ($P = 0.00002$) and between PHANToM and Rehab ($P = 0.0075$) indicate that the mean of WFs is significantly lower for RHI and PHANToM in comparison to that for Rehab.

One reason for the same performance achieved with the RHI and the PHANToM is that the PHANToM has itself

Table III. Mean and Std values for the experiment measures for each HI

	RHI	PHANToM	Rehab
WF (%)	0.111 (std=0.019)	0.118 (std=0.021)	0.145 (std=0.021)
JND (N/m)	5.571 (std=0.916)	5.953 (std=1.068)	7.205 (std=1.024)
PSE (N/m)	50.035 (std=0.578)	50.238 (std=1.695)	49.654 (std=1.267)

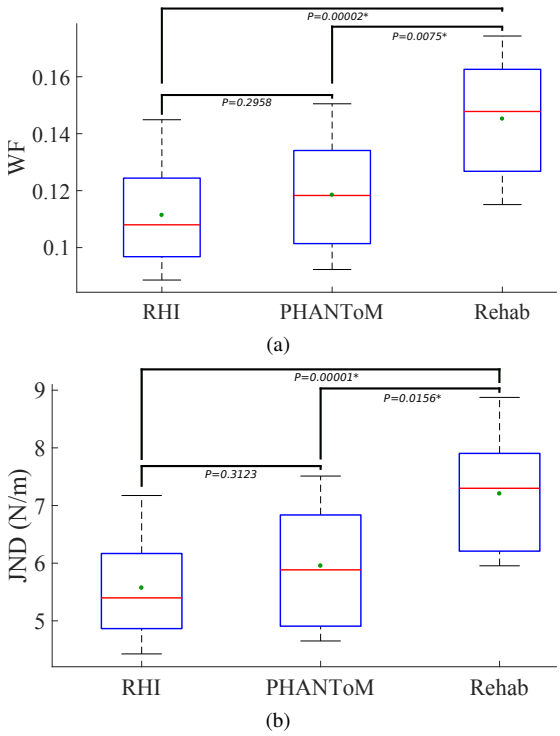

Figure 7. (a) WF, and (b) JND . The median and mean values are shown with red line and green circle, respectively.

small friction and apparent inertia [35], and the difference between the performance of the RHI and the PHANToM lies below the sensitivity threshold of the human hand for stiffness sensing. However, as can be seen in Fig 4, the added kinematics redundancy to the base of the PHANToM solves the comparatively small workspace problem of the PHANToM. Having a small workspace requires the user to use the clutching mechanism to move the EE of the HI to another position or orientation in the workspace (e.g., in the middle of the workspace) [36]; clutching is required in a master-slave system where the slave's workspace is significantly bigger than the master's. This will slow down the user to perform a task. As for the Rehab, it was observed that its relatively large apparent inertia and friction make it hard for the human subjects to perceive the difference between two soft tissues that have close stiffness value.

VI. Conclusion and Future Work

In this paper, we compared users' performance for a soft-tissue stiffness discrimination task using redundant and non-redundant haptic interfaces. Our goal was to study how a redundant haptic interface (RHI) can be used to decrease

the apparent inertia and increase the manipulability of the human interface, and consequently improve the resolution of force feedback for the user. We conducted a set of perceptual experiments to evaluate how different HIs affect the perception of virtual stiffnesses for human users. Experimental results demonstrate that the RHI leads to better sensitivity in discriminating between stiffness of two tissue samples. In this paper, a virtual environment is used to set up a haptic interaction system with nearly-ideal transparency and without any communication delay to show the advantages of an RHI over the NHIs in terms of stiffness discrimination. In the future, the teleoperated master-slave system will be used to investigate the effectiveness of the proposed system in teleoperated systems. In the future, we will perform more experiments to statistically evaluate the performance of the RHI for different reference stimuli values and investigate the performance of the RHI for both soft- and hard-tissues. Here it is assumed that the direction of the movement, u, is known to the secondary objective controller. However, in the future works, the direction of the movement or the intention of the user will be found by using machine learning methods (e.g. Hidden Markov Model) and/or by measuring the torque/force applied by the user's hand on the haptic interface. In the future, we will investigate how the minimum number of added DoFs for a desired improvement in manipulability, apparent inertia, and JND can be attained.

REFERENCES

[1] G. Sutherland, S. Lama, L. S. Gan, S. Wolfsberger, and K. Zareinia, "Merging machines with microsurgery: clinical experience with neuroArm." *Journal of neurosurgery*, vol. 118, no. 3, pp. 521–9, 2013.

[2] B. Hannaford and A. M. Okamura, "Haptics," in *Springer Handbook of Robotics*, B. Siciliano and O. Khatib, Eds. Springer International Publishing, 2016, pp. 1063–1084.

[3] A. D. Greer, P. M. Newhook, and G. R. Sutherland, "Human–machine interface for robotic surgery and stereotaxy," *IEEE/ASME Transactions on Mechatronics*, vol. 13, no. 3, pp. 355–361, 2008.

[4] M. Tavakoli, R. V. Patel, and M. Moallem, "A haptic interface for computer-integrated endoscopic surgery and training," *Virtual Reality*, vol. 9, no. 2-3, pp. 160–176, 2006.

[5] M. Tavakoli, A. Aziminejad, R. Patel, and M. Moallem, "High-fidelity bilateral teleoperation systems and the effect of multimodal haptics," *IEEE Transactions on Systems, Man and Cybernetics – Part B*, vol. 37, no. 6, pp. 1512–1528, December 2007.

[6] H. Mayer, I. Nagy, A. Knoll, E. U. Braun, R. Bauernschmitt, and R. Lange, "Haptic feedback in a telepresence system for endoscopic heart surgery," *Presence: Teleoperators and Virtual Environments*, vol. 16, no. 5, pp. 459–470, 2007.

[7] T. Yamamoto, N. Abolhassani, S. Jung, A. M. Okamura, and T. N. Judkins, "Augmented reality and haptic interfaces for robot-assisted surgery," *The International Journal of Medical Robotics and Computer Assisted Surgery*, vol. 8, no. 1, pp. 45–56, 2012.

[8] M. V. Ottermo, M. Øvstedal, T. Langø, Ø. Stavdahl, Y. Yavuz, T. A. Johansen, and R. Mårvik, "The role of tactile feedback in laparoscopic surgery," *Surgical Laparoscopy Endoscopy & Percutaneous Techniques*, vol. 16, no. 6, pp. 390–400, 2006.

[9] R. L'Orsa, C. J. Macnab, and M. Tavakoli, "Introduction to haptics for neurosurgeons," *Neurosurgery*, vol. 72, no. Supplement, pp. A139–A153, 2013.

[10] V. Hayward and O. R. Astley, "Performance Measures for Haptic Interfaces," *International Symposium In Robotics Research*, vol. 1, pp. 195–207, 1996.

[11] B. Siciliano, "Kinematic control of redundant robot manipulators: A tutorial," *Journal of Intelligent and Robotic Systems*, vol. 3, no. 3, pp. 201–212, 1990.

[12] M. Ueberle, N. Mock, and M. Buss, *Design, Control, and Evaluation of a Hyper-redundant Haptic Device*. Berlin, Heidelberg: Springer Berlin Heidelberg, 2007, pp. 25–44.

[13] N. Nath, E. Tatlicioglu, and D. M. Dawson, "Teleoperation with kinematically redundant robot manipulators with sub-task objectives," *Robotica*, vol. 27, pp. 1027–1038, 2009.

[14] A. Barrow and W. Harwin, "Design and analysis of a haptic device design for large and fast movements," *Machines*, vol. 4, no. 1, pp. 1–19, 2016.

[15] F. Gosselin, C. Andriot, F. Bergez, and X. Merlhiot, "Widening 6-dof haptic devices workspace with an additional degree of freedom," in *Second Joint EuroHaptics Conference and Symposium on Haptic Interfaces for Virtual Environment and Teleoperator Systems (WHC'07)*, March 2007, pp. 452–457.

[16] J. K. Salisbury Jr, A. J. Madhani, G. S. Guthart, G. D. Niemeyer, and E. F. Duval, "Master having redundant degrees of freedom," Patent US 6,684,129, Jan. 27, 2004.

[17] D.-Y. Hwang and B. Hannaford, "Teleoperation performance with a kinematically redundant slave robot," *The International Journal of Robotics Research*, vol. 17, no. 6, pp. 579–597, 1998.

[18] H. Das, T. B. Sheridan, and J. J. E. Slotine, "Kinematic control and visual display of redundant teleoperators," in *Conference Proceedings., IEEE International Conference on Systems, Man and Cybernetics*, Nov 1989, pp. 1072–1077 vol.3.

[19] T. Yoshikawa, "Manipulability of Robotic Mechanisms," *The International Journal of Robotics Research*, vol. 4, no. 2, pp. 3–9, 1985.

[20] B. Siciliano, L. Sciavicco, L. Villani, and G. Oriolo, *Robotics - Modelling, Planning and Control*. Springer-Verlag London, 2009.

[21] O. Khatib, "A unified approach for motion and force control of robot manipulators: The operational space formulation," *IEEE Journal on Robotics and Automation*, vol. 3, no. 1, pp. 43–53, February 1987.

[22] O. Khatib, "Inertial Properties in Robotic Manipulation: An Object Level Framework," *International Journal Of Robotics Research*, vol. 13, no. 1, pp. 19–36, 1995.

[23] J. Nakanishi, R. Cory, M. Mistry, J. Peters, and S. Schaal, "Operational space control: A theoretical and empirical comparison," *International Journal of Robotics Research*, vol. 27, no. 6, pp. 737–757, 2008.

[24] M. Sharifi, H. Salarieh, S. Behzadipour, and M. Tavakoli, "Impedance control of non-linear multi-dof teleoperation systems with time delay: absolute stability," *IET Control Theory Applications*, vol. 12, no. 12, pp. 1722–1729, 2018.

[25] S. Sra, "A new metric on the manifold of kernel matrices with application to matrix geometric means," in *Advances in Neural Information Processing Systems*. Curran Associates, Inc., 2012, pp. 144–152.

[26] M. C. Çavuşoğlu, D. Feygin, and F. Tendick, "A critical study of the mechanical and electrical properties of the phantom haptic interface and improvements for highperformance control," *Presence: Teleoperators and Virtual Environments*, vol. 11, no. 6, pp. 555–568, Dec 2002.

[27] M. D. Dyck, "Measuring the Dynamic Impedance of the Human Arm," M.Sc. Thesis, University of Alberta, 2013.

[28] G. A. Gescheider, *Psychophysics: The fundamentals, 3rd ed.* Mahwah, NJ, US: Lawrence Erlbaum Associates Publishers, 1997.

[29] P. Schiavone, F. Chassat, T. Boudou, E. Promayon, F. Valdivia, and Y. Payan, "In vivo measurement of human brain elasticity using a light aspiration device," *Medical Image Analysis*, vol. 13, no. 4, pp. 673 – 678, 2009.

[30] A. M. Okamura, "Methods for haptic feedback in teleoperated robot-assisted surgery," *Industrial Robot: An International Journal*, vol. 31, no. 6, pp. 499–508, 2004.

[31] F. A. Wichmann and N. J. Hill, "The psychometric function: I. fitting, sampling, and goodness of fit," *Perception & Psychophysics*, vol. 63, no. 8, pp. 1293–1313, Nov 2001.

[32] G. D. Gersem, H. V. Brussel, and F. Tendick, "Reliable and enhanced stiffness perception in soft-tissue telemanipulation," *The International Journal of Robotics Research*, vol. 24, no. 10, pp. 805–822, 2005.

[33] F. Tendick, M. C. Cavusoglu, N. Dhruv, and A. Sherman, "Maximizing the sensation of compliance in teleoperative surgery," in *Intl. Symp. Robotics with Applications (ISORA)*, 2000.

[34] E. Karadogan, R. L. Williams, J. N. Howell, R. R. Conatser Jr *et al.*, "A stiffness discrimination experiment including analysis of palpation forces and velocities," *Simulation in Healthcare*, vol. 5, no. 5, pp. 279–288, 2010.

[35] T. H. Massie and J. K. Salisbury, "The phantom haptic interface: A device for probing virtual objects," in *Proceedings of the ASME Dynamic Systems and Control Division*, 1994, pp. 295–301.

[36] K. Zareinia, Y. Maddahi, C. Ng, N. Sepehri, and G. R. Sutherland, "Performance evaluation of haptic hand-controllers in a robot-assisted surgical system," *The International Journal of Medical Robotics and Computer Assisted Surgery*, vol. 11, no. 4, pp. 486–501, dec 2015.